

Magnetic and electronic structure of $(\text{Ga}_{1-x}\text{Mn}_x)\text{As}$

L. Bergqvist,¹ P. A. Korzhavyi,² B. Sanyal,¹ S. Mirbt,¹ I. A. Abrikosov,¹ L. Nordström,¹ E. A. Smirnova,³ P. Mohn,⁴ P. Svedlindh,⁵ and O. Eriksson¹

¹*Department of Physics, Uppsala University, Box 530, SE-75121, Uppsala, Sweden*

²*Department of Materials Science, Royal Institute of Technology, SE-100 44 Stockholm, Sweden*

³*Department of Theoretical Physics, Moscow Institute of Steel and Alloys, 119991 Moscow, Russia*

⁴*Center for Computational Materials Science, TU Wien, A-1060 Wien, Austria*

⁵*Department of Materials Science, Uppsala University, Box 530, SE-75121, Uppsala, Sweden*

(Received 5 November 2002; published 6 May 2003)

We present theoretical calculations of the magnetic and electronic structure of Mn-doped GaAs (in the zinc-blende structure). The magnetic properties are shown to be very sensitive to structural defects, in particular, As antisite defects and Mn at interstitial positions. Only when considering such defects can the experimental magnetic moments be reproduced by first-principles theory. We present a simple model for understanding the connection between the magnetic ordering and the As antisites, and the way in which the defects help to stabilize a partial disordered local-moment state. The connection between the energetics of the Mn substitution and the As antisite concentration is also analyzed. In addition, we compare the calculated magnetic properties and electronic structures of Mn situated on substitutional sites (Mn replacing a Ga atom) and on interstitial sites, where in agreement with observations the interstitial site is found to be less favorable. Finally, combining our first-principles calculations of the spin-wave excitation energies with a classical Heisenberg Hamiltonian we have calculated interatomic exchange interactions, and using Monte Carlo simulations we present theoretical values of the critical temperature as a function of Mn concentration.

DOI: 10.1103/PhysRevB.67.205201

PACS number(s): 75.25.+z, 75.70.-i, 85.75.-d

I. INTRODUCTION

Dilute magnetic semiconductors are argued to be of scientific and technological importance,¹ e.g., due to applications in spin electronics.² Substitution of Mn for Ga in GaAs, forming $\text{Mn}_x\text{Ga}_{1-x}\text{As}$ with Mn concentrations up to 10%, has been shown to result in a particularly promising material. Although the magnetic structure and critical temperature are known to be sensitive to the way in which the samples have been prepared, e.g., annealing conditions, etc., one can conclude that in favorable cases a critical temperature of ~ 100 K has been observed.^{1,3,4} Quite recently it was also shown that Mn implanted in GaP can in very specific cases have a critical temperature close to room temperature.⁵ The fact that the magnetic properties are affected by the annealing suggests that there may be lattice defects and/or inhomogeneities in the samples, and arsenic antisite defects (denoted As_{Ga}) have been observed.⁶ Due to a high equilibrium vapor pressure of As, epitaxial growth of GaAs is usually performed at a certain As overpressure that produces an As-rich GaAs.⁷ Combined with the high concentration of Mn atoms (which act as acceptors), such experimental conditions make the formation of As antisites (which act as donors) energetically favorable. In the work of Ref. 6 it was also shown that the As_{Ga} are connected to a local lattice deformation that can be as large as $\sim 10\%$ in the bond length. The replacement of Mn for Ga is shown to result in a small lattice distortion around the Mn atom, deduced both from experimental⁸ and theoretical⁹ techniques. Also, the electronic properties of $\text{Mn}_x\text{Ga}_{1-x}\text{As}$ have been studied using optical probes¹⁰ and by angle-resolved photoemission.¹¹ The magnetic properties of $\text{Mn}_x\text{Ga}_{1-x}\text{As}/\text{GaAs}/\text{Mn}_x\text{Ga}_{1-x}\text{As}$ trilayers have been measured, with an unexpected large interlayer exchange con-

stant and a proposed metallic behavior of the GaAs spacer.¹²

The intense experimental efforts to understand these materials are paralleled with equally intense theoretical efforts. Hence both the electronic structure and magnetic properties of defect-free Mn-GaAs have been studied.^{9,13-24} In addition, the transport properties of $\text{Mn}_x\text{Ga}_{1-x}\text{As}/\text{GaAs}$ heterostructures have been calculated using first-principles theory.²⁵ The origin of the ferromagnetism in these systems is under discussion, and models including the Ruderman-Kittel-Kasuya-Yosida model,¹⁴ the competition between the double- and superexchange mechanisms,¹³ and a double-resonance mechanism¹⁵ have been proposed. First-principles calculations on defect-free Mn-GaAs give total magnetic moments of $4\mu_B/\text{Mn}$ atom for ferromagnetically coupled Mn impurities on the Ga sublattice in GaAs.^{9,18,21-24} This result is in sharp contrast to the experimental results obtained by saturation magnetization measurements that are significantly smaller, $2.4\mu_B/\text{Mn}$ atom.²⁶ This marked disagreement between experimental saturation magnetization data and the theory was recently argued by us²⁶ to be due to As antisite defects.²⁷ By considering the presence of As_{Ga} , theory showed that a disordered local-moment (DLM) state²⁸ minimized the total energy. This state has *only a part* of the randomly distributed Mn atoms ferromagnetically aligned while *the remaining fraction* of the Mn atoms has an orientation of their magnetic moments antiparallel to the global magnetization direction, and this magnetic configuration reproduced the observed macroscopic magnetic moment with good accuracy. We remark here that subsequently a different mechanism involving spin disorder of the Mn atoms with a spin-glass-type structure has been proposed.²⁹ Other defect structures have also been suggested and, in particular, Mn atoms situated at interstitial positions have been detected³⁰

and argued to be of importance regarding the magnetic properties.

In order to facilitate a technological breakthrough using magnetic semiconductors with a critical temperature above room temperature, an understanding of their magnetic properties and a correlation to the electronic structure must be achieved, and for this reason it is interesting to investigate the electronic and magnetic structure of Mn-doped GaAs. In this paper we give a full account of our theoretical data for the $(\text{Ga}_{1-x}\text{Mn}_x)\text{As}$ system, involving the electronic and magnetic structure of defect-free samples and of samples with As antisites. We also present theoretical data for the phase stability of these materials, both in the presence of antisites and without lattice defects. Finally we present calculations of the critical temperatures of defect-free $(\text{Ga}_{1-x}\text{Mn}_x)\text{As}$, showing that in the defect-free limit it should be possible to fabricate dilute magnetic semiconductors with critical temperatures close to room temperature.

II. THEORY

The electronic structure and total-energy calculations for disordered $(\text{Ga}_{1-x-y}\text{Mn}_x\text{As}_y)\text{As}$ alloys were based on the density-functional theory³¹ and we made use of the local-density approximation.³² We employed a basis set of the linear muffin-tin orbitals^{33,34} (LMTO) with $l_{\max}=2$, in conjunction with the multipole-corrected atomic sphere approximation (ASA).³⁵ The dependence of the results on the cutoff or the exchange-correlation potential used in our calculations have been checked and found to be negligible. We used equal Wigner-Seitz sphere radii for all the atoms on the Ga and As sublattices, as well as for the empty spheres representing the two types of interstitial sites in the zinc-blende structure of GaAs. The substitutional and magnetic disorder on the Ga sublattice was treated within the coherent-potential approximation (CPA).³⁶ In these calculations the Mn atoms were allowed to have collinear, but random spin-up or spin-down orientations of their local spin moments by means of the DLM model.²⁸ In our theoretical treatment we have minimized the total energy with respect to the fraction of the $\text{Mn}\uparrow$ and $\text{Mn}\downarrow$ atoms, and the system may obtain a ferromagnetic component in a state that is intermediate between a saturated ferromagnetic state and a paramagnetic DLM state.³⁷

The LMTO-CPA calculations were augmented with supercell calculations using a noncollinear tight-binding LMTO-ASA (TB-LMTO-ASA) method³⁸ as well as a full potential LMTO (FP-LMTO) method.³⁹ The noncollinear TB-LMTO-ASA calculations used the local-density approximation³² and included the combined correction terms in the one-electron Hamiltonian. Calculations were based on a supercell approach where one Ga atom was replaced by a Mn atom. The concentration of Mn depends on the size of the supercell. We have studied spin-wave excitations based on the adiabatic treatment of the magnetic moments and used the so-called frozen magnon approach.^{40–44} In this approach, the total energy $E(\mathbf{q}, \theta)$ of spiral magnetic structures is calculated and each atomic spin direction is defined by the Euler angles

$$\theta_i = \text{const}; \quad \phi_i = \mathbf{q} \cdot \mathbf{R}_i, \quad (1)$$

where θ_i and ϕ_i are the polar and azimuthal angles, \mathbf{R}_i the position of ion i , and \mathbf{q} is the spiral propagation vector. Because of the generalized translational periodicity of spin spirals,⁴⁵ the calculations can be performed in the chemical unit cell for all spirals without the need for a larger supercell. Spin-wave excitation energies are given by the relation

$$\omega(\mathbf{q}) = \frac{4}{M} \frac{\Delta E(\mathbf{q}, \theta)}{\sin^2 \theta}, \quad (2)$$

where $\Delta E(\mathbf{q}, \theta) = E(\mathbf{q}, \theta) - E(0, \theta)$. In all calculations, we used $\theta = 45^\circ$, choose spirals along high-symmetry directions in the Brillouin zone, and calculated the total-energy self-consistently.

A generalized Heisenberg Hamiltonian of classical spins was used to describe the interactions between the magnetic ions,

$$H = - \sum_{i \neq j} J_{ij} \mathbf{e}_i \cdot \mathbf{e}_j - \sum_{i \neq j} K_{ij} (\mathbf{e}_i \cdot \mathbf{e}_j)^2, \quad (3)$$

where J_{ij} and K_{ij} are exchange parameters and are obtained by least-squares fitting of the spiral energies.⁴¹

The critical temperatures were estimated both from Monte Carlo (MC) simulations and the mean-field approximation (MFA). We used the standard single flip Metropolis algorithm in the MC simulations and determined the critical temperatures using the “cumulant crossing method.”⁴⁶ We then calculated the reduced fourth-order cumulant of the order parameter (magnetization) U_L , defined as

$$U_L = 1 - \frac{\langle M^4 \rangle}{3 \langle M^2 \rangle^2}, \quad (4)$$

for different lattice sizes. The curves of U_L will have a common intersection at a fixed point U^* , which will be the critical point. Hence, we obtained a value of T_c from the intersection point of U_L for different lattice sizes.

In the calculations, we used a simulation box of size $L \times L \times L$ with periodic boundary conditions. The linear lattice size L has been varied from 16 to 48. The total number of MC steps/spin were around 20 000 where the averages of the thermodynamic observables were measured in the last 15 000 steps.

In the MFA, the critical temperature is given by the relation

$$k_B T^{MFA} = \frac{2}{3} \sum_j J_{0j}. \quad (5)$$

For the FP-LMTO calculations the LDA exchange-correlation functional (von Barth–Hedin parametrization) was used. In the FP-LMTO method the unit cell is divided into nonoverlapping muffin tin spheres and the interstitial region. The basis functions are linearized muffin-tin orbitals with quantum numbers (n, l, m) and also the tail energy κ^2 . The angular part of such a basis function is a Y_{lm} spherical harmonic. The radial part is a numerically calculated function inside the muffin tin and Hankel or Neumann function in

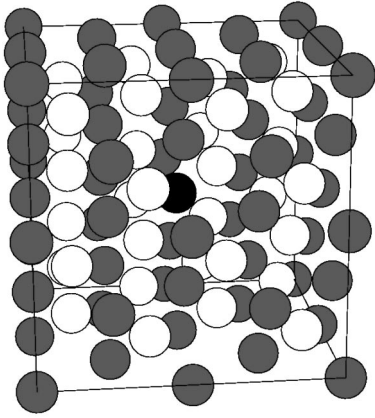


FIG. 1. Supercell (64 atoms) used in some of the calculations. The gray circles represent Ga atoms and the white circles the As atoms, whereas the substituting Mn atom is shown as a black circle.

the interstitial region. The potential and the charge density are expanded in spherical harmonics up to $l_{max}=6$ in the muffin-tin region and in a Fourier series in the interstitial region, therefore there is no shape approximation to the potential or charge density. All the electrons in the crystal are divided into core and valence states. For our calculations the basis set included Mn $4s, 4p$, and $3d$ states; Ga $4s, 4p, 3d$, and $4d$ states; and As $4s, 4p, 3d$, and $4d$ states. All other electron states were treated as core states. We used a double basis set, i.e., two basis functions with different tail energies for each (n, l, m) .

Before we describe our results we show in Fig. 1 one of the supercells used in our calculations. Several sizes of the supercell were used, corresponding to 8, 16, 32, and 64 atoms (Mn concentrations of $x=0.25$, $x=0.125$, $x=0.0625$, and $x=0.03125$, respectively), but we choose to display only the largest cell. All supercells used are cubic and have symmetry of a simple cubic lattice for the 8- and 64-atom supercells, fcc for 16 atoms, and bcc for the 32-atom cell. The distance between nearest-neighbor Mn atoms in the four supercells is therefore a , $\sqrt{2}a$, $\sqrt{3}a$, and $2a$, where a is the lattice parameter of GaAs.

III. RESULTS

A. Electronic and magnetic structure of $(\text{Ga}_{1-x}\text{Mn}_x)\text{As}$

In Fig. 2 we show the density of states (DOS) for ferromagnetic (FM) $(\text{Ga}_{0.96}\text{Mn}_{0.04})\text{As}$ without As antisites [Fig. 2(a)] and with As antisites [Fig. 2(b)]. From this figure one may observe that the spin-up Mn- d states form a rather wide (~ 5 eV) band, which is due to the degeneracy and corresponding hybridization with the GaAs valence band.

The spin-down Mn- d states are located in the band-gap region. Hence the hybridization is substantially lower, which results in a much narrower structure with a width of ~ 1.5 eV. There are, however, spin-down Mn- d states that hybridize with the GaAs valence band, as is visible from the figure. Since without antisite defects the DOS shows half-metallic behavior (a band gap at the Fermi level, E_F , for the spin-down states) the total magnetic moment must be an in-

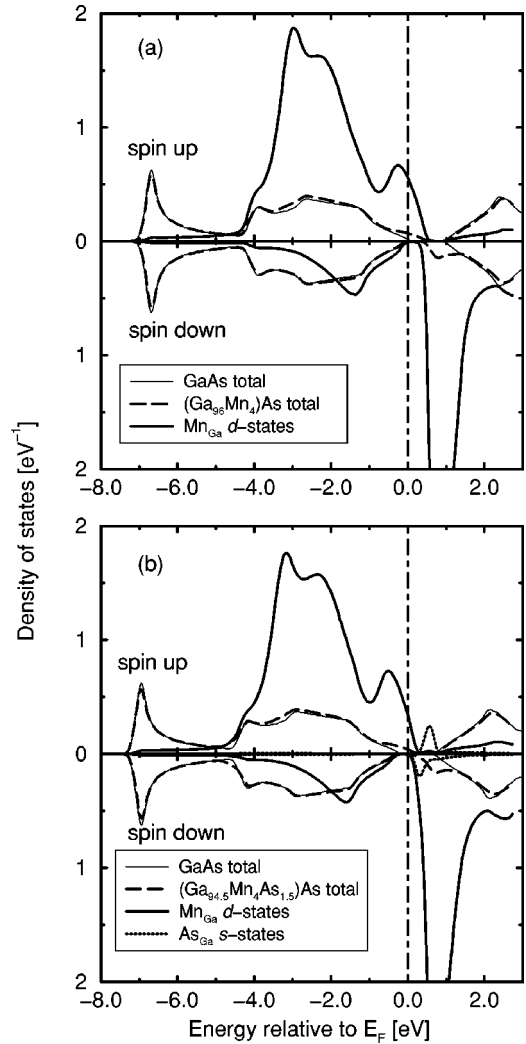


FIG. 2. Calculated DOS of $(\text{Ga}_{1-x}\text{Mn}_x)\text{As}$ in the FM state, (a) without As antisites and (b) with As antisites. The Mn- d states are shown on an expanded scale.

teger. Our calculations hence result in a total moment of $4\mu_B/\text{Mn}$ atom, although the moment projected onto the atomic sphere of the Mn atom is noninteger. The presence of As antisites [Fig. 2(b)] does not seem to affect the overall features of the electronic structure. The main differences are that E_F shifts to somewhat higher values to accommodate the extra electrons associated with the defects and the appearance of an As- s state in the band gap. This state is actually quite important for the magnetic coupling and we will return to it below.

In Fig. 3(a) we show the electron density of a smaller supercell with eight atoms/unit cell. The electron density was calculated with a full potential method and the density is shown for a cut in the 110 plane. The corresponding magnetization density is shown in Fig. 3(b). The general shape of the densities shown in Fig. 3 is also found for lower Mn concentrations (larger supercell sizes) and for this reason they are not displayed. As can be seen, almost all the magnetization density is located around the Mn atom, which is natural since this atom carries the main part of the magnetic

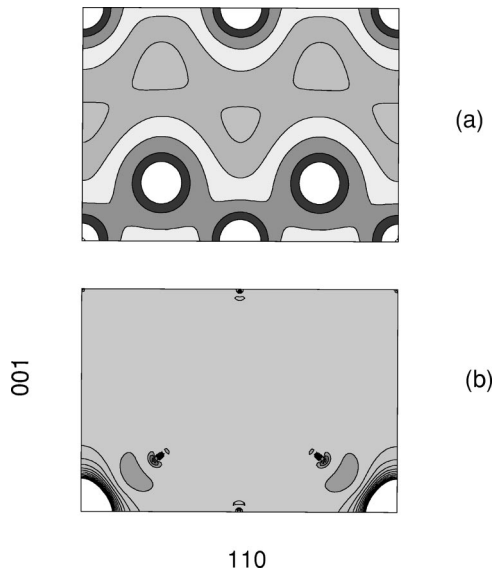


FIG. 3. (a) Calculated charge and (b) spin density of a $(\text{Ga}_7\text{Mn}_1)\text{As}_8$ supercell in the zinc-blende structure and in the FM state. The plane is defined by the 001 and 110 vectors. The calculations were made with the FP-LMTO method. The Mn atoms are positioned at the lower corners of the figure, whereas the remaining atoms along the edges are Ga atoms. All other atoms are As atoms.

moment. The charge density shows a somewhat more surprising result, in that the Mn atom can hardly be distinguished from the Ga atoms, with electron lobes connecting the atoms. For a Ga atom in GaAs this is expected since the electron density follows the sp^3 hybrids. Replacing Ga for Mn is expected to destroy these hybrids and the covalent bonding and should hence be visible in the charge density. However, as Fig. 3(a) shows the charge density around a Mn atom is actually quite reminiscent of an sp^3 bonded system.

Next, we consider the magnetic properties and the total energy of the DLM state. In our theory we calculated the total energy for different fractions of Mn atoms aligned parallel and antiparallel to the global magnetization direction. This calculation was repeated for different values of As antisites. In Fig. 4 we display the calculated net magnetization as a function of the As_{Ga} concentration, determined for the magnetic configurations which minimize the total energy of the DLM state.²⁶ Without antisite defects, theory gives a total magnetic moment of $4\mu_B/\text{Mn}$ atom in agreement with previous theory but in disagreement with experiment. As may be seen in the figure the original increase of the total magnetization as a function of antisite concentration is followed by a sharp drop of the average magnetic moment at As_{Ga} concentrations above 1%. In our previous report²⁶ we proposed that the As_{Ga} concentration is 1.7%. Note that for this As_{Ga} concentration the theoretical calculations (Fig. 4) result in a magnetization that is in very good agreement with the experimental values²⁶ ($\sim 2.4\mu_B/\text{Mn}$ atom). Hence, when allowing the system to form a partial DLM state the magnetic ordering produces a theoretical magnetic moment that is in agreement with experiment. We also find that the degree of spin disorder, i.e., the fraction between the number of spin-down and spin-up Mn atoms, is heavily dependent on the

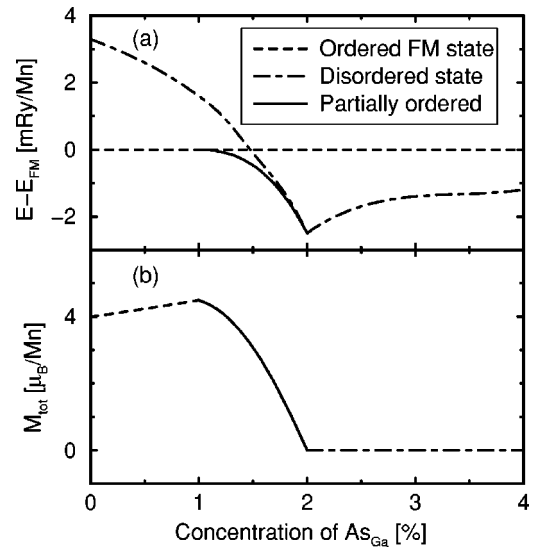


FIG. 4. (a) Energies of completely disordered and partially ordered configurations of local moments on Mn atoms in $(\text{Ga}_{96-x}\text{Mn}_4\text{As}_x)\text{As}$, relative to energy of the fully ordered (ferromagnetic) state, as a function of the As antisite concentration. (b) Total spin magnetic moment of $(\text{Ga}_{96-x}\text{Mn}_4\text{As}_x)\text{As}$ in the lowest-energy state. The legend applies to both panels.

As_{Ga} concentration, and that the magnetic properties of this system hence are very sensitive to the defects of the lattice. It should be noted, however, that the size of the magnetic moments of the different individual Mn atoms is large for all As_{Ga} concentrations (of the order of $4\mu_B$ – $4.5\mu_B$).

B. A model for the influence of antisite defects on the magnetic structure

In order to understand the origin of a formation of the DLM state in $(\text{Ga}_{1-x}\text{Mn}_x)\text{As}$ it is relevant to analyze the electronic structure of these materials and the way in which it depends on As_{Ga} concentration. Let us consider a simple model of the density of states (DOS) shown in Fig. 5. In the figure we show the Mn- d states and the valence and conduction bands of GaAs, as well as the deep impurity level introduced by As_{Ga} antisites. The Mn- d orbitals have the majority states located at the top of the valence band and the minority states at the bottom of the conduction band. The Fermi level cuts through the majority states but lies in the gap of the minority states, yielding a half-metallic material. We remark that this model is in accord with our self-consistent calculations (Fig. 2), as well as with other first-principles calculations for ferromagnetic $(\text{Ga}_{1-x}\text{Mn}_x)\text{As}$.^{18,20}

If one considers GaAs (without Mn) in the presence of As antisites, each As_{Ga} impurity is associated with two extra electrons that occupy an impurity level situated in the band gap. The presence of the As antisites hence gives rise to a spin degenerate impurity level in the band gap that accommodates two electrons, one spin up and one spin down. This is indeed the situation in $(\text{Ga}_{1-x}\text{Mn}_x)\text{As}$, as illustrated in Fig. 5. If the material is in a ferromagnetic state the spin-up electron can lower its energy from the impurity level to E_F , whereas the spin-down electron cannot, since there are no

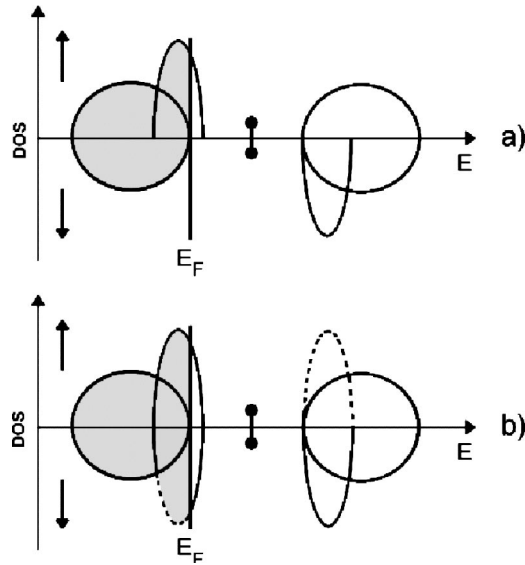


FIG. 5. Simple model of the electronic structure (DOS) of $(\text{Ga}_{1-x}\text{Mn}_x)\text{As}$ in the (a) FM and (b) DLM states. The valence and conduction bands of GaAs are marked by broad semiovals and the Mn- d states are indicated as narrow states at the top of the valence band (with filled lines for the $\text{Mn}\uparrow$ atoms and dashed lines for the $\text{Mn}\downarrow$ atoms in DLM state) and the bottom of the conduction band. The impurity state due to the As antisites lies in the band gap and is marked by a single discrete level occupied by two electrons (indicated by two filled dots). The spin-up (-down) states are marked with an arrow pointing up (down).

available empty states in the spin-down band (one could, of course, consider an As_{Ga} defect with a spin triplet impurity state, but the energy of such a state is considerably higher than the spin degenerate impurity). If the material forms a DLM state the electronic structure is changed so that both spin-up and -down Mn- d states are located at the top of the valence band (see Fig. 5). Hence, both the spin-up and spin-down electrons of the As_{Ga} impurity level can in this case lower the total energy by filling low-energy Mn- d states. Thus, in the presence of As_{Ga} impurities, we have identified a driving mechanism that favors a transition from the saturated ferromagnet to the DLM magnetic state.

It remains to determine why the FM state is the ground state in the absence of the antisite defects. In Fig. 6 we present the calculated DOS of $(\text{Ga}_{0.96}\text{Mn}_{0.04})\text{As}$ (with and without As_{Ga} atoms) in the DLM configuration at which a small (0.25%) fraction of Mn atoms have flipped their magnetic moments against the total magnetization direction. In the figure the DOS is shown for the Mn atoms that are aligned in the opposite direction of the global magnetization direction. Without As_{Ga} antisites the $\text{Mn}\downarrow$ - d states form a very narrow impurity subband that is situated exactly at the Fermi level, an energetically very unfavorable situation. Therefore, a flip of a Mn local moment in $(\text{Ga}_{0.96}\text{Mn}_{0.04})\text{As}$ from a ferromagnetic to a DLM configuration is energetically very costly, which is why the Mn atoms order ferromagnetically. The presence of As antisites in $(\text{Ga}_{0.945}\text{Mn}_{0.04}\text{As}_{0.015})\text{As}$ changes the situation. The impurity subband of the $\text{Mn}\downarrow$ atoms is now entirely below the Fermi

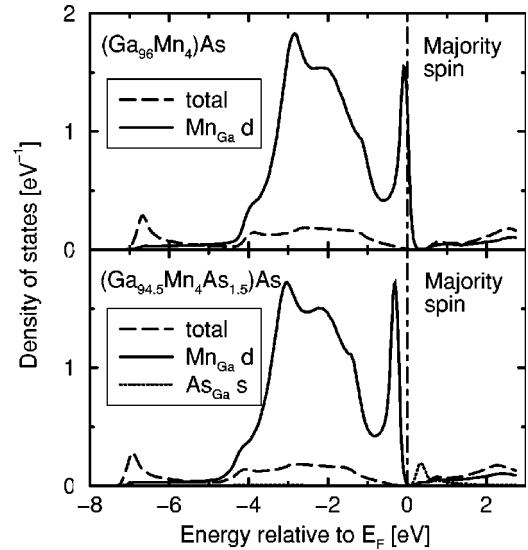


FIG. 6. Majority d -projected DOS of $(\text{Ga}_{1-x}\text{Mn}_x)\text{As}$ in the DLM state with (lower panel) and without (upper panel) As antisite defects. Only the spin-down states of Mn atoms aligned opposite the global magnetization direction are shown. The Mn- d states are shown on an expanded scale.

level, due to the band filling effect driven by the As antisites. This reduces the energy cost of the DLM state, compared to the ferromagnetic state and together with the discussion regarding Fig. 5 it explains the coupling between As defects and magnetic ordering in these materials.

C. Effect of interstitial Mn

So far, we have considered only the substitutional Mn (Mn_S) atoms in the Ga sites. In the experimental samples, a certain percentage of Mn is found to occupy also interstitial positions. Yu *et al.*³⁰ have performed experiments to show the presence of interstitial Mn (Mn_I) atoms and the correlation between the Curie temperature, T_C , and different Mn sites. Maca and Masek⁴⁷ carried out electronic structure calculations to show a comparison between the substitutional and interstitial Mn atoms. It was found that an interstitial Mn atom acts as a donor and it compensates the holes produced by substitutional Mn atoms. This is reflected in the lowering of T_C . In Fig. 7, we show a comparison between the calculated⁴⁸ densities of states of Mn_S and Mn_I atoms, for the compositions of $\text{MnGa}_{15}\text{As}_{16}$ and $\text{MnGa}_{16}\text{As}_{16}$, respectively. It is seen from the figure that Mn- d states in the spin-up channel are considerably different for Mn_S and Mn_I . The main peak is 2.5 eV below the Fermi level for Mn_S and 1 eV below for Mn_I .

For Mn_S the Fermi level lies in the gap of the spin-down states and is situated at the top of the valence band of the spin-up states. For Mn_I the situation is reversed in the sense that the Fermi level lies at the bottom of the conduction band of the spin-down states. We also note that the shape of the projected DOS is different for the two configurations. For Mn_S there is a strong hybridization between Mn- d and GaAs- sp states, which results in a wide band. For Mn_I this

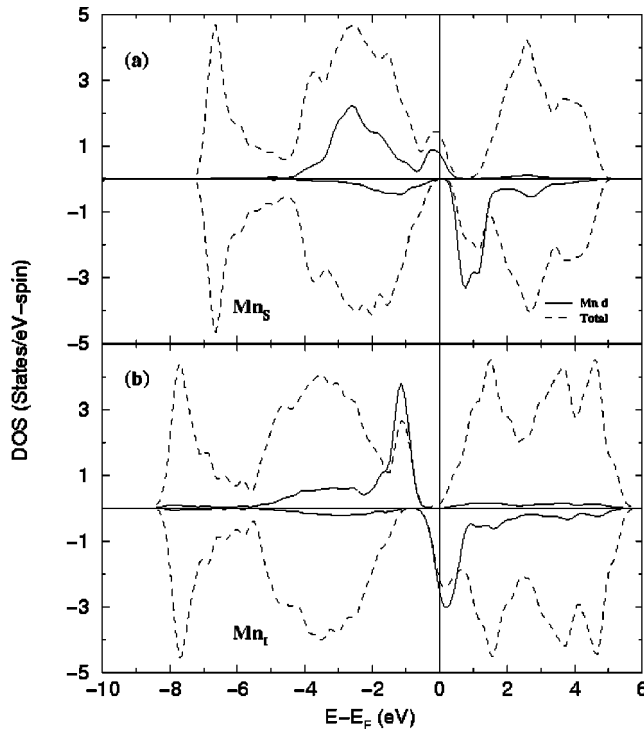


FIG. 7. DOS of $(\text{Ga}_{1-x}\text{Mn}_x)\text{As}$ with Mn atoms in (a) substitutional and (b) interstitial position. The total DOS of the unit cell is shown as a dashed line and the Mn- d -projected DOS as a full line, on an expanded scale.

hybridization is much lower, resulting in a much narrower Mn- d DOS. The exchange splitting for Mn_I is seen to be less than that of Mn_S .

The total moment in the interstitial case is reduced to $3.06\mu_B/\text{cell}$ compared to $4.00\mu_B/\text{cell}$ in the substitutional case. Partial magnetic moments on the Mn site are $3.58\mu_B$ and $2.82\mu_B$ for Mn_S and Mn_I , respectively. The reduction of the magnetic moment is due to the partial filling of the spin-down Mn- d band. Interstitial Mn acts as a double donor which is evident from the occupancy of the conduction band. As a donor, Mn_I can compensate holes associated with, for instance, substitutional Mn atoms. Also, the half metallicity is destroyed as the Fermi level crosses both the spin-up and spin-down bands. We calculated the formation energies of neutral Mn defects in the two cases and found that the interstitial Mn defect has an energy approximately 1 eV higher than the substitutional one. This is consistent with the fact that usually Mn sites are identified in experiments as substitutional.

A complete compensation occurs for a configuration of one Mn_I and two Mn_S atoms in the unit cell. First, we calculated the exchange interaction between a Mn_S and a Mn_I atom in a $\text{Mn}_2\text{Ga}_{15}\text{As}_{16}$ unit cell by comparing the total energies of ferromagnetic (FM) and antiferromagnetic (AFM) alignment of the two Mn spins. The AFM alignment is lower in energy by an amount of 0.15 eV/Mn atom. To simulate complete compensation, we put two Mn_S atoms and one Mn_I atom in the $\text{Mn}_3\text{Ga}_{14}\text{As}_{16}$ unit cell and calculated the energy differences between FM and two different AFM couplings between the Mn atoms. In the first calculation we considered

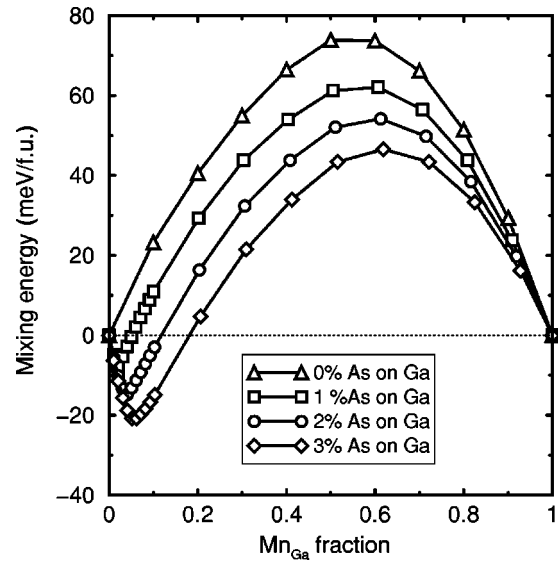


FIG. 8. Mixing energy of $(\text{Ga}_{1-x}\text{Mn}_x)\text{As}$ as a function of the Mn concentration. The calculated values are shown for different concentrations of As antisites.

AFM coupling between the two Mn_S atoms. The energy of this configuration is 0.09 eV/Mn-atom lower than the FM case. In the second calculation we considered ferromagnetically coupled Mn_S atoms that are aligned antiferromagnetically to the Mn_I atom. The energy of this configuration was 0.19 eV/Mn-atom lower than the ferromagnetic coupling.

One can understand the AFM ordering between Mn_S and Mn_I using similar arguments to those of the As antisite induced DLM ordering. As Fig. 7 shows, the donor electrons of the Mn_I atom are of spin-down d character, whereas available acceptor levels of the Mn_S atom have spin-up d character. In order for compensation to occur (which lowers the total energy) the coupling between Mn_S and Mn_I must be antiferromagnetic.

D. Phase stability of $(\text{Ga}_{1-x}\text{Mn}_x)\text{As}$

In Fig. 8 we show the calculated mixing energy, i.e., the energy difference $E[(\text{Ga}_{1-x}\text{Mn}_x)\text{As}] - xE(\text{MnAs}) - (1-x)E(\text{GaAs})$, where all systems were in the zinc-blende structure. It is important to note that the ground-state structure of MnAs is not the zinc-blende structure, but rather the NiAs structure. Our calculations show that MnAs in the NiAs structure has a lower energy than it has in the zinc-blende structure by approximately 1 eV/f.u. Hence Fig. 8 does not show the true mixing energy. However, it is nevertheless interesting to study the energy difference in the zinc-blende structure shown in Fig. 8, since zinc-blende MnAs can be stabilized as overlayers or in superlattices with GaAs. Figure 8 shows that in the absence of As antisites the mixing energy is positive for all Mn concentrations.

In the presence of As antisites the mixing energy is negative for certain Mn concentrations. The lowest energy is always found at Mn and As antisite concentrations that correspond to complete compensation, i.e., when the hole of the Mn atom is filled by the two extra electrons of the As anti-

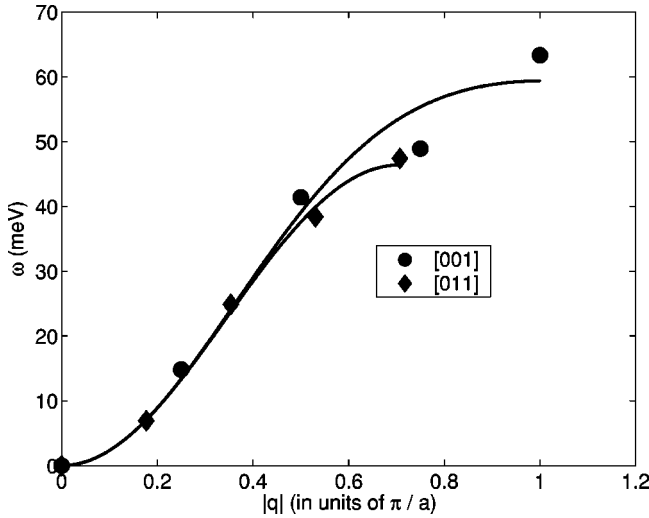


FIG. 9. Spin-wave excitation spectrum of $(\text{Ga}_{15}\text{Mn}_1)\text{As}_{16}$ along the 001 and 011 directions.

site. This means that for a Mn concentration of, e.g., 6%, complete compensation occurs for a concentration of 3% As antisites. That this balance between concentrations is favored is not very surprising since in this case all of the impurity electrons can lower their energy by filling valence-band holes.

As we have shown in a previous paper²⁶ complete compensation is, from a practical viewpoint, not desired since the total magnetic moment of the DLM state in this case is zero. We end this subsection by noting that the data in Fig. 8 may explain why it is possible to grow MnAs in the zinc-blende structure and $(\text{Ga}_{1-x}\text{Mn}_x)\text{As}$ for values of x lower than $\sim 12\%$, since for intermediate concentrations the calculations result in too large and positive mixing energies.

E. Critical temperature of defect-free $\text{Ga}_{1-x}\text{Mn}_x\text{As}$

The calculated spin-wave energies for $(\text{Ga}_{1-x}\text{Mn}_x)\text{As}$ with concentration of $x = 0.0625$ are presented in Fig. 9 to-

gether with fitted values [Eqs. (2) and (3)]. We used exchange interactions up to five nearest neighbor shells of Mn atoms which gave reasonably good agreement with calculated energies. We choose to show the results only for an Mn concentration of $x = 0.0625$ but the results look similar for the other concentrations.

Results from Monte Carlo simulations are shown in Fig. 10. Note that the results of magnetization and especially susceptibility are plagued with finite-size effects. Here we are mainly interested in critical temperature which we extract from the fourth-order cumulant U_L [Eq. (4)]. In this way, the finite-size errors cancel completely at the critical point and we therefore do not need the critical exponents. However, for a more careful study around the critical point, for instance, a calculation of correlation functions, the critical exponents are indeed needed and can be calculated from finite-size scaling theory.

The calculated critical temperatures are presented in Fig. 11. Both mean-field and MC results give similar dependencies of the critical temperature but MC calculations always give lower values because they take into account fluctuations which are absent in the MFA. The critical temperatures agree rather well with those in Ref. 24 based on the random-phase approximation. Calculated values are substantially higher than experimental ones which are around 110 K for $x = 0.05$. The most likely explanation for this difference is the presence of antisites and other defects in the experimental samples. In addition, the Mn atoms in our simulations are also ordered, while in the materials studied experimentally they are disordered. The critical temperature increases with increasing Mn concentrations but has a maximum at $x = 0.125$ and decreases at higher concentrations in qualitative agreement with experiments⁴⁹ (which show a maximum at $x \approx 0.05$).

IV. SUMMARY

We have presented theoretical calculations of the magnetic and electronic structure of Mn-doped GaAs and found

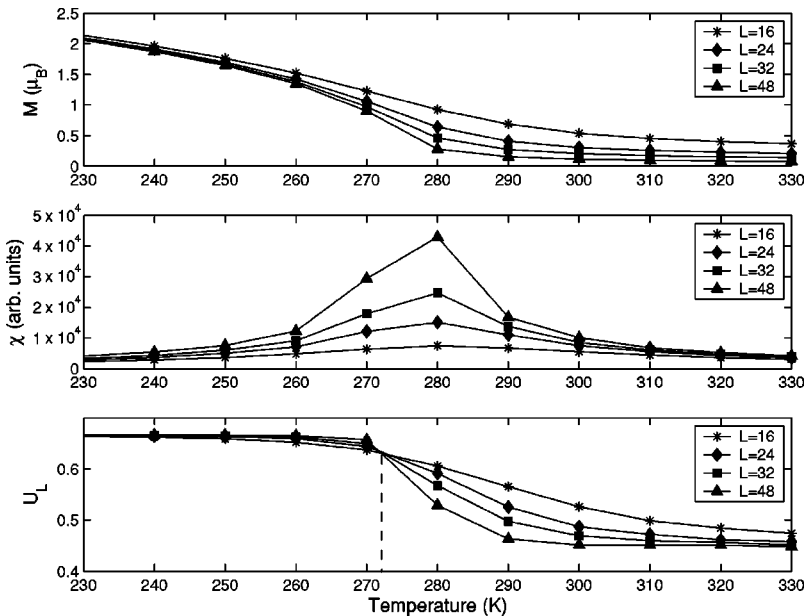


FIG. 10. Magnetic moment (M), susceptibility (χ), and fourth-order cumulant (U_L) as a function of temperature for different sizes of the simulation box.

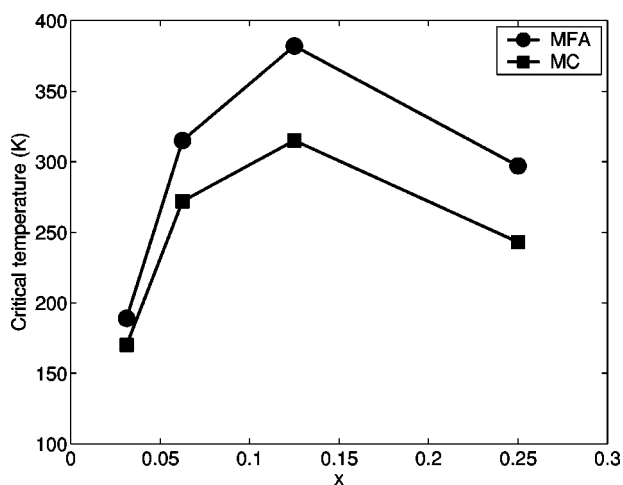


FIG. 11. Calculated values of the critical temperature of $(\text{Ga}_{1-x}\text{Mn}_x)\text{As}$ as a function of Mn concentration (x). The calculations were based on Monte Carlo simulations (MC) as well as the mean-field approximation (MFA) (see text) and were carried out for ideal, defect free samples.

that the magnetic properties are very sensitive with respect to structural defects, in particular, As antisite defects and Mn interstitial defects. Only when considering such defects can the experimental magnetic moments be reproduced by first-principles theory. We present a simple model for understanding the connection between the magnetic ordering and the As antisites, and the way in which the defects help stabilize a DLM state. The connection between the energetics of the Mn substitution and the As antisite concentration is also analyzed and we find that a complete compensation is the most favored situation. In addition we analyze the spin and charge density around the Mn atoms inside the GaAs host material. We also compare the calculated magnetic properties and electronic structures of Mn situated on substitutional sites (Mn replacing a Ga atom) and on interstitial sites, where in agreement with observations the interstitial site is found to

be less favorable. Also, by combining our first-principles calculations of the spin-wave excitation energies with a classical Heisenberg Hamiltonian we have calculated the interatomic exchange interactions. Using Monte Carlo simulations we obtained theoretical values of the critical temperature as a function of Mn concentration and we find that the maximum value is found for $\sim 12\%$. In addition we show that critical temperatures derived from mean-field theory give consistently higher values than those from Monte Carlo.

Finally, we have shown that the magnetic moments and critical temperatures of magnetically doped semiconductors could be increased substantially by elimination of defects, putting high demands on the film preparation of these materials. Indeed, recent experiments⁵⁰ show that the saturation magnetization increases when the $(\text{Ga}_{1-x}\text{Mn}_x)\text{As}$ films are annealed at low temperature, which might support the picture given in the present report. One might also speculate that an elimination of the electrons of the As-s impurity state by, e.g., light-induced excitations or an applied electric field could alter the magnetic ordering and strengthen the ferromagnetic coupling, which would possibly increase the critical temperature and magnetic moment.

ACKNOWLEDGMENTS

We acknowledge support from the Swedish Research Council (VR) and the Swedish Foundation for Strategic Research (SSF). The collaboration between Sweden and the former Soviet Union was supported by The Royal Swedish Academy of Sciences. The Swedish Foundation for International Cooperation in Research and Higher Education (STINT) is gratefully acknowledged. Support from the National Supercomputer Center (NSC) is acknowledged. P.M. is grateful to the RTN Network, Contract No. HPRN-CT-2000-00143, Computational Magneto-electronics for support. O.E. is grateful to the Göran Gustafsson Foundation for support.

- ¹H. Ohno, *Science* **281**, 951 (1998); Y. Ohno, D.K. Young, B. Beschoten, F. Matsukura, H. Ohno, and D.D. Awschalom, *Nature (London)* **402**, 790 (1999); H. Ohno, D. Chiba, F. Matsukura, T. Omiya, E. Abe, T. Dietl, Y. Ohno, and K. Ohtani, *ibid.* **408**, 944 (2000).
- ²G. Prinz, *Science* **282**, 1660 (1998); J. de Boeck and G. Borghs, *Phys. World* **12**, 27 (1999).
- ³H. Ohno, A. Shen, F. Matsukura, A. Oiwa, A. Endo, S. Katsumoto, and Y. Iye, *Appl. Phys. Lett.* **69**, 363 (1996).
- ⁴B. Beschoten, P.A. Crowell, I. Malajovich, D.D. Awschalom, F. Matsukura, A. Shen, and H. Ohno, *Phys. Rev. Lett.* **83**, 3073 (1999).
- ⁵N. Theodoropoulou, A.F. Hebard, M.E. Overberg, C.R. Abernathy, S.J. Pearton, S.N.G. Chu, and R.G. Wilson, *Phys. Rev. Lett.* **89**, 107203 (2002).
- ⁶T.E.M. Staab, R.M. Nieminen, J. Gebauer, R. Krause-Rehberg, M. Luysberg, M. Haugk, and Th. Frauenheim, *Phys. Rev. Lett.*

- 87**, 045504 (2001); M. Kaminska, Z. Liliental-Weber, E.R. Weber, T. George, J.B. Kortright, F.W. Smith, B.-Y. Tsaur, and A.R. Calawa, *Appl. Phys. Lett.* **54**, 1881 (1989); X. Liu, A. Prasad, J. Nishio, E.R. Weber, Z. Liliental-Weber, and W. Walukiewicz, *ibid.* **67**, 279 (1995).
- ⁷R.M. Cohen, *Mater. Sci. Eng.*, **20**, 167 (1997).
- ⁸Y.L. Soo, S.W. Huang, Z.H. Ming, Y.H. Kao, H. Munekata, and L.L. Chang, *Phys. Rev. B* **53**, 4905 (1996).
- ⁹M. Jain, L. Kronik, J.R. Chelikowsky, and V.V. Godlevsky, *Phys. Rev. B* **64**, 245205 (2001).
- ¹⁰E.J. Singley, R. Kawakami, D.D. Awschalom, and D.N. Basov, *Phys. Rev. Lett.* **89**, 097203 (2002).
- ¹¹J. Okabayashi, A. Kimura, O. Rader, T. Mizokawa, A. Fujimori, T. Hayashi, and M. Tanaka, *Phys. Rev. B* **64**, 125304 (2001).
- ¹²W. van Roy, H. Akinaga, and S. Miyashashi, *Phys. Rev. B* **63**, 184417 (2001).
- ¹³H. Akai, *Phys. Rev. Lett.* **81**, 3002 (1998).

- ¹⁴T. Dietl, H. Ohno, F. Matsukura, J. Cibert, and D. Ferrand, *Science* **287**, 1019 (2000); T. Dietl, H. Ohno, and F. Matsukura, *Phys. Rev. B* **63**, 195205 (2001).
- ¹⁵J. Inoue, S. Nonoyama, and H. Itoh, *Phys. Rev. Lett.* **85**, 4610 (2000).
- ¹⁶J. König, H.H. Lin, and A.H. MacDonald, *Phys. Rev. Lett.* **84**, 5628 (2000).
- ¹⁷J. Schliemann, J. König, H.H. Lin, and A.H. MacDonald, *Appl. Phys. Lett.* **78**, 1550 (2001).
- ¹⁸S. Sanvito, P. Ordejon, and N.A. Hill, *Phys. Rev. B* **63**, 165206 (2001).
- ¹⁹Y.-J. Zhao, W.T. Geng, K.T. Park, and A.J. Freeman, *Phys. Rev. B* **64**, 035207 (2001).
- ²⁰S. Mirbt, B. Sanyal, and P. Mohn, *J. Phys.: Condens. Matter* **14**, 3295 (2002).
- ²¹A. Zunger, in *Solid State Physics*, edited by H. Ehrenreich and D. Turnbull (Academic, New York, 1986), Vol. 39.
- ²²M. Schilfsgaarde and O.N. Mryasov, *Phys. Rev. B* **63**, 233205 (2001).
- ²³E. Kulatov, H. Nakayama, H. Mariette, H. Ohta, and Yu.A. Usenskii, *Phys. Rev. B* **66**, 045203 (2002).
- ²⁴L. Sandratskii and P. Bruno, *Phys. Rev. B* **66**, 134435 (2002).
- ²⁵S. Sanvito and N.A. Hill, *Phys. Rev. Lett.* **87**, 267202 (2001).
- ²⁶P.A. Korzhavyi, I.A. Abrikosov, E.A. Smirnova, L. Bergqvist, P. Mohn, R. Mathieu, P. Svedlindh, J. Sadowski, E.I. Isaev, Yu.Kh. Vekilov, and O. Eriksson, *Phys. Rev. Lett.* **88**, 187292 (2002).
- ²⁷B. Grandidier, J.P. Nys, C. Delerue, D. Stiévenard, Y. Higo, and M. Tanaka, *Appl. Phys. Lett.* **77**, 4001 (2000).
- ²⁸B.L. Gyorffy, A.J. Pindor, J.B. Staunton, G.M. Stocks, and H. Winter, *J. Phys. F: Met. Phys.* **15**, 1337 (1985).
- ²⁹G. Zarand and B. Janko, *Phys. Rev. Lett.* **89**, 047201 (2002).
- ³⁰K.M. Yu, W. Walukiewicz, T. Wojtowicz, I. Kuryliszyn, X. Liu, Y. Sasaki, and J.K. Furdyna, *Phys. Rev. B* **65**, 201303 (2002).
- ³¹P. Hohenberg and W. Kohn, *Phys. Rev.* **136**, B864 (1964); W. Kohn and L.J. Sham, *Phys. Rev.* **140**, A1133 (1965).
- ³²J.P. Perdew, K. Burke, and M. Ernzerhof, *Phys. Rev. Lett.* **77**, 3865 (1996). In the present work, we have not used the gradient corrections.
- ³³O.K. Andersen, *Phys. Rev. B* **12**, 3060 (1975); O.K. Andersen and O. Jepsen, *Phys. Rev. Lett.* **53**, 2571 (1984).
- ³⁴The semicore 3d states on Ga were treated as valence states. Therefore, instead of using the LMTO parametrization of the potential function, we calculated its exact energy dependence.
- ³⁵H.L. Skriver and N.M. Rosengaard, *Phys. Rev. B* **46**, 7157 (1992); P.A. Korzhavyi, I.A. Abrikosov, B. Johansson, A.V. Ruban, and H.L. Skriver, *ibid.* **59**, 11 693 (1999).
- ³⁶See J.S. Faulkner, *Prog. Mater. Sci.* **27**, 1 (1982), for a review, and A.V. Ruban, I.A. Abrikosov, and H.L. Skriver, *Phys. Rev. B* **51**, 12 958 (1995), for the details of the CPA method. The Madelung potential and energy contributions due to charge fluctuations in the alloy were evaluated within the screened impurity model (SIM), P.A. Korzhavyi, A.V. Ruban, I.A. Abrikosov, and H.L. Skriver, *ibid.* **51**, 5773 (1995). The SIM effective screening radius, $R_{eff} \approx 0.4a$ (where a is the lattice parameter), and the Madelung energy prefactor, $\beta = 0.5$, were chosen on the basis of supercell calculations.
- ³⁷H. Akai and P.H. Dederichs, *Phys. Rev. B* **47**, 8739 (1993).
- ³⁸This program is a development of the method published by N. Rosengaard and B. Johansson, *Phys. Rev. B* **55**, 14 975 (1997). For details see L. Bergqvist, L. Nordström, and O. Eriksson (unpublished) (www.fysik.uu.se/theomag).
- ³⁹J. M. Wills, O. Eriksson, M. Alouani, and D. L. Price, in *Electronic Structure and Physical Properties of Solids: The Uses of the LMTO Method*, edited by H. Dreyse (Springer, Berlin, 1998).
- ⁴⁰A.I. Liechtenstein, M.I. Katsnelson, V.P. Antropov, and V.A. Gubanov, *J. Magn. Magn. Mater.* **67**, 65 (1987).
- ⁴¹N.M. Rosengaard and B. Johansson, *Phys. Rev. B* **55**, 14 975 (1997).
- ⁴²M. Uhl and J. Kübler, *Phys. Rev. Lett.* **77**, 334 (1996).
- ⁴³S.V. Halilov, H. Eschrig, A.Y. Perlov, and P.M. Oppeneer, *Phys. Rev. B* **58**, 293 (1998).
- ⁴⁴M. Pajda, J. Kudrnovsky, I. Turek, V. Drchal, and P. Bruno, *Phys. Rev. B* **64**, 174402 (2001).
- ⁴⁵L.M. Sandratskii, *Adv. Phys.* **47**, 1 (1998).
- ⁴⁶D. P. Landau and K. Binder, *A Guide to Monte Carlo Simulations in Statistical Physics* (Cambridge University, Cambridge, England, 2000).
- ⁴⁷F. Maca and J. Masek, *Phys. Rev. B* **65**, 235209 (2002).
- ⁴⁸G. Kresse and J. Hafner, *Phys. Rev. B* **47**, 558 (1993); G. Kresse and J. Furthmüller, *ibid.* **54**, 11 169 (1996).
- ⁴⁹F. Matsukura, H. Ohno, A. Shen, and Y. Sugawara, *Phys. Rev. B* **57**, 2037 (1998).
- ⁵⁰S.J. Potashnik, K.C. Ku, S.H. Chun, J.J. Berry, N. Samarth, and P. Schiffer, *Appl. Phys. Lett.* **79**, 1495 (2001).